Evidence for Long-Range Coulomb Effects during Formation of Nanoparticle Agglomerates from Pyrolysis and Combustion Routes†

5 AUTHORS, INCLUDING:

Vladimir Vasil`evich Karasev
Russian Academy of Sciences
41 PUBLICATIONS   277 CITATIONS

SEE PROFILE

Vladimir Alkseevich Strunin
Russian Academy of Sciences
67 PUBLICATIONS   501 CITATIONS

SEE PROFILE

Evidence for Long-Range Coulomb Effects during Formation of Nanoparticle Agglomerates from Pyrolysis and Combustion Routes[†]

A. A. Onischuk,*,‡ S. di Stasio,§ V. V. Karasev,‡ V. P. Strunin,‡ A. M. Baklanov,‡ and V. N. Panfilov‡

Institute of Chemical Kinetics and Combustion, Siberian Branch of the Russian Academy of Sciences, 630090, Novosibirsk, Russia and Istituto Motori C.N.R. Fluid Dynamics and Combustion Division, Via Marconi 8−80125 Napoli, Italy

Two processes of the agglomeration of aerosol particles are investigated. The first process involves silicon aerosol formation by silane pyrolysis in a flow reactor. In the second process, soot aerosol is formed during propane combustion in a Bunsen burner. The agglomerate size and morphology are analyzed by a transmission electron microscope. An imaging system is used to observe agglomerate−agglomerate coagulation and agglomerate sticking to the deposit formed on the surface (tendrils). The movement of agglomerates in the electric field is also studied using the imaging system. It is found that Coulomb interactions are significant during the sticking process and, in particular, they are responsible for the fractal dimension, inferred in the experiments to be significantly lower with respect to the values obtainable from diffusion limited cluster−cluster aggregation simulations. However, the mechanism of this interaction is different for silicon and soot agglomeration processes. It is found that the silicon agglomerates are dipoles with net charges equal to zero. By contrast, approximately half of the soot agglomerate population is estimated to be charged with a net charge equal to one elementary unit (positive or negative). The major result is that the Coulomb interactions are observed to hold considerable influence during the process of agglomerate−agglomerate sticking, in particular, encouraging the agglomerate mutual sticking at the tips of the single agglomerates.

1. Introduction

Agglomeration of aerosol nanoparticles is a phenomenon that frequently occurs in different natural and industrial processes. The single subunits, which stick together and form larger clusters, are called primary particles, monomers, or spherules. Several experimental contributions in the literature report on the agglomerate formation for titania,[1−7] silica,[1,5,8−10] and soot[11−13] nanoparticles in temperature driven chemical reactions. All of the above agglomeration processes are schematized to be composed of similar stages. First, nucleation takes place resulting in small particle formation. Then, coagulation coupled with coalescence occurs. At the initial stage of the process, coalescence dominates, giving rise to approximately spherical particles. Then, the rate of coalescence became lower than the coagulation rate. As a result, agglomerates of primary particles are formed. These agglomerates have a loose irregular structure, which can be described in terms of fractal dimension $D_f < 3$ through the following power law expression that links the agglomerate mass M and size R with the size a of spherules, respectively:

$$M \propto (R/a)^{D_f} \qquad (1)$$

Our knowledge of the agglomeration mechanism is much improved by numerical simulations[11,14−25] which usually predict a fractal dimension $D_f = 1.7−1.9$ for the cluster−cluster

diffusion limited agglomeration (CCDLA). A number of experimental works are in agreement with these theoretical predictions. However, some experimental investigations give considerably smaller values of fractal dimensions than the calculated D_f for DLCCA process. Thus, Samson et al.[11] measured $D_f = 1.5−1.6$ for soot agglomerates, Hurd and Flower[8] obtained $D_f \approx 1.5$ for silica agglomerates, Rogak et al.[7] derived $D_f = 1.45−1.66$ for silicon agglomerates, Rogak et al.[6] obtained $D_f = 1.3−1.6$ for TiO_2 agglomerates. di Stasio[12,13] measured $D_f = 1.25−1.8$ for soot agglomerates in diffusion propane-air and ethylene-air flames at atmospheric pressure. The most probable explanation of these low values of D_f is to assume the existence of long-range interactions between coagulating particles.[8,14,17] This assumption is supported by several papers,[26−31] which report about charged soot agglomerates formed in combustion processes. Thus, for example, Ball and Howard[26] measured the electric charge of carbon particle agglomerates formed in premixed propane−oxygen flame. The authors concluded that the agglomerates contained from 200 to 14000 positive charges (1 to 40 charges per primary particle). No negative charges were found. Wersborg et al.[27] investigated the electric charge of soot agglomerates formed in premixed acetylene−oxygen flame. The number fraction of charged particles is 10 to 40%. The amount of charge was found to be 1 or 2 elementary units per agglomerate. Place and Weinberg[29] studied the electrical characteristics of carbon formation for a flat counter-flow diffusion flame. In this case, the authors reported that all of the carbon particles are charged. There are a few papers[28−31] that discuss the possibility of positive ions serving as nuclei for soot particle growth.

Evidence for Long-Range Coulomb Effects

J. Phys. Chem. A, Vol. 104, No. 45, 2000 **10427**

The aim of the present paper is to report the direct experimental evidence of a significant influence by the Coulomb interactions on the agglomeration mechanisms and, consequently, on the fractal dimension D_f of growing clusters. Two different agglomerate processes are considered, namely, the formation of silicon agglomerates under the silane pyrolysis and of soot agglomerates during propane combustion. In the two cases, the effects of Coulomb interactions are investigated, and the results are compared. An estimation of the dipole moments obtained on the basis of the experimental results for both silicon and soot agglomerates is also reported.

2. Experiments

2.1. Silane Pyrolysis. Silane pyrolysis was carried out using a vertical flow reactor with an inner diameter of 1.1 cm.[32] A mixture of silane with argon was supplied to the inlet of reactor. The reactor temperature was in the range 800−950 K. The reaction time was varied in the range 0.2−1.0 s by changing flow rate of the gas mixture coming through the reactor. Under-decomposed silane, gaseous intermediates (disilane, trisilane, hydrogen, and others), and agglomerates of aerosol particles were coming out of the outlet of reactor.[32] These agglomerates were sampled downstream by a thermophoretic technique for the Transmission Electron Microscopy (TEM) analysis performed by the microscope JEM 100SX.

Aerosol particles formed due to silane pyrolysis consist of amorphous hydrogenated silicon.[33,34] The hydrogen content in the particles was measured by the hydrogen evolution method.[33,35,36] To this end, the aerosol particles were sampled by a quartz filter. The deposited mass was determined by weighing. Then the filter was placed into a small chamber connected with a mass-spectrometer. The temperature of the sample was increased with a constant rate of 33 K/min. During this heating, the hydrogen component evolved to the gas phase. Experimental data were represented as hydrogen evolution rate vs heating temperature. Three characteristic peaks were observed in the hydrogen evolution spectra. Two relatively narrow peaks with maxima near 670 and 760 K are caused by the evolution from polyhydride groups $(SiH_2)_n$ and monohydride groups SiH localized inside of the amorphous silicon networks, respectively. The third peak, which was relatively broad with respect to the previous ones, is at about 780 K and corresponds to the hydrogen evolution from SiH groups localized at the surface of interconnected micro-voids and microchannels. When the heating temperature was about 950 K the crystallization of the sample occurred and all the hydrogen was released to the gas phase. Thus, the hydrogen evolution method gives information on the total number of bonded hydrogen atoms and the number of SiH and $(SiH_2)_n$ groups in the sample.

To observe the coagulation of silicon agglomerates in real time, an imaging system was used. To this aim, a portion of the aerosol was injected to an optically accessible volume lighted by a He−Ne laser beam. The light scattered by the aerosol agglomerates at the angle 90° is collected by a micro-objective lens and then gathered to a CCD camera connected to a TV system. This optical setup allowed for the resolution of images of agglomerate size larger than about 3 μm. Smaller agglomerates were visible only as fuzzy spots. The movement of these spots in the presence of electric field gave information on the electric charge and dipole moment of the single agglomerates.

2.2. Soot Analysis. Soot was formed in a combustion process. A Bunsen burner is fuelled with pure propane (99.99%). As is well-known, the Bunsen burner is made by an inner tube (diameter 10 mm), inside which the fuel (propane) flows from
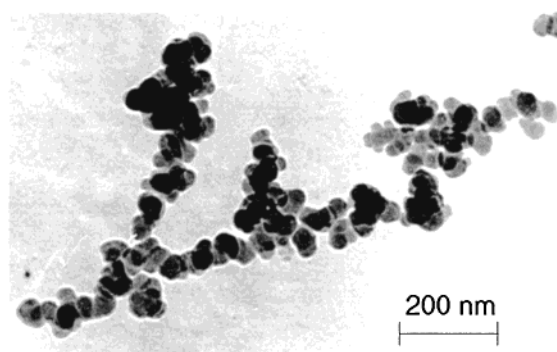

Figure 1. Agglomerates of silicon aerosol particles formed by silane pyrolysis at $T = 853$ K. Reaction time, $t_r = 0.5$ s, cold-zone coagulation time (downstream) $t_c = 10$ s.

a bottle. At the base of the burner, there is a duct connecting the bottle directly to the inner tube. At the same time, a movable ring co-annular to the central tube, can be positioned in a way to more or less permit air entrainment from ambient. Inside the inner tube, the air and fuel gas flow upstream and mix together, owing to molecular transport (diffusion). Thus, the airflow inside the inner tube is strongly dependent upon the position of the windowed ring. At the rim of the burner, a flame composed of two different colored zones can be observed. At the mouth of the burner, a conical flame of bluish color is observed. This is produced by the combustion of the air−fuel mixture gas flowing in the inner tube, which can be considered as a premixed fuel-rich laminar flame, so that the composition of the burned gas does not correspond with complete combustion. By rotating the annular ring at the base of the burner, it is possible to augment the air entrainment and the height of the bluish flame. The second observed flame portion is of yellow appearance (with a high concentration of larger soot particles inside), and it surrounds the bluish cone (where nucleation of soot particles occurs). The yellow flame portion is roughly conical with a larger section in the lower part and a more sharpened top part, and it can be considered to be a diffusion flame between the gas from the inner flame, which contains excess of gaseous hydrocarbons, and the surrounding air.

In our case, the air inlet ring at the base of the burner is blocked in such a way to ensure a minimum (nonzero) air entrainment in the lower part of the inner tube. This is made with the aim of making the flame configuration reproducible. The position of this annular windowed ring corresponds to the most flame rich condition of the inner diffusion flame portion at the burner rim. Thus, the height of the bluish zone is at its minimum (about 4−5 mm). The flow rate of propane entering the base of the burner was about 4 cm³/s. The apparent total length of the generated flame was 12−14 cm. For the TEM analysis, soot was sampled at different heights above burner (HABs) using a specially created probing system. The aerosol was sampled by a probe positioned on the flame axis. The probe was constituted by a capillary duct (i.d. = 0.06 cm, length = 5 cm) with a flow rate of 0.5 cm³/s. At the capillary outlet, the flow was diluted by a factor of 400 with filtered air. Then, the aerosol was sampled by a vacuum impactor onto an electron microscopy grid covered by polyvinyl Formvar film.

The soot samples destined to the on-line imaging system were carried out from the overflame region at HAB = 14 cm.

3. Results

3.1. Silicon Agglomerates. Figure 1 shows an example of an agglomerate of aerosol particles formed by silane pyrolysis.
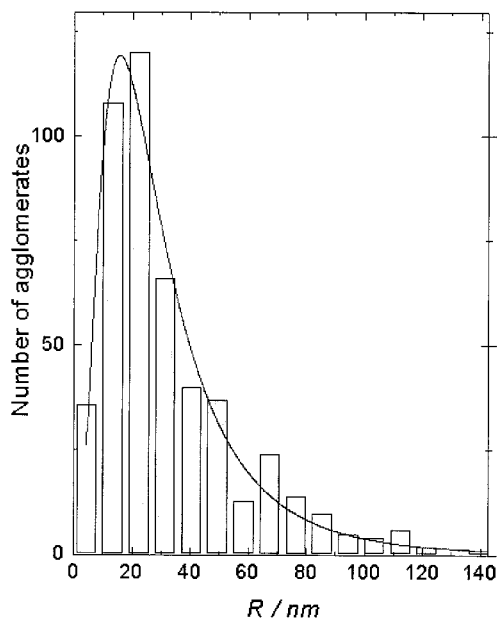
Figure 2. Frequency distribution of silicon agglomerate radii R. Reaction time, $t_t = 0.2$ s. Cold-zone coagulation is suppressed.

The agglomerate consists of small primary particles of $10-50$ nm in size. To describe the size of agglomerates, we introduce the radius R, following the approach of Samson et al.[11]

$$R = \frac{1}{2} \sqrt{LW} \qquad (2)$$

where L is the maximum length of the agglomerate image, and W is the maximum extension of the agglomerate perpendicular to L. After being removed from the reactor, the aerosol particles were subjected to a coagulation process in the cold zone downstream during time t_c. The radius of the agglomerates increased from 0.1 to 1 μm, with t_c increasing from 6 to 100 s. The mean ratio L/W did not depend on the cold zone coagulation time and was equal to $L/W \approx 1.9$ for the whole range $6 < t_c < 100$ s. Figure 2 shows a frequency distribution of agglomerate radius R, which is well modeled by a log-normal size distribution function of the type

$$f(R) = (R\sqrt{2\pi} \ln \sigma_g)^{-1} exp\left\{-\left[\frac{(\ln R/R_0)^2}{2(\ln \sigma_g)^2}\right]\right\} \qquad (3)$$

with $\sigma_g = 2.0$; R_0 is geometric mean radius.

The fractal dimension was determined from the analysis of the TEM micrographs. As preliminary step, an estimation of the agglomerate volumes was given. Thus, the agglomerates under consideration were partitioned into several sections. To estimate the volume of the parts constituting each agglomerate, these sub-constituents were approximated by spheres, cylinders, or ellipsoids of revolution. As a rule, the overlapping subunits were sufficiently distinguished in the micrographs. Therefore, we suppose that this method of estimation of the agglomerate volume V is satisfactory, although we use 2D projections. Then, the fractal dimension was determined from the log-log plots of V vs R. More than 100 agglomerates were proceeded for each plot. Two regimes of agglomeration were investigated from the point of view of fractal dimension. The first regime corresponded to the condition that the reaction time ($t_R = 0.2-0.9$ s) was much higher than the coagulation time t_c observed in the cold zone of the reactor (downstream). To enter this regime, the aerosol flow was diluted by a factor 50 with pure
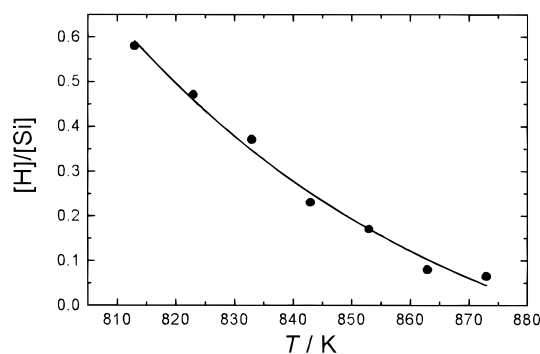

Figure 3. The ratio [H]/[Si] of the total number of hydrogen atoms to the number of silicon atoms in aerosol particles vs reactor temperature.
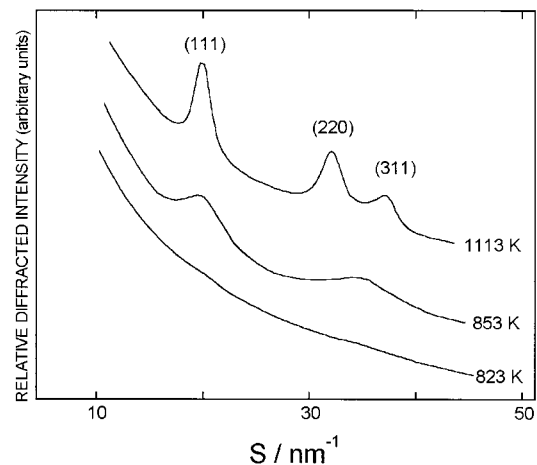

Figure 4. Scattered electron intensity profiles from sampled silicon agglomerates. Data were obtained by TEM in the regime of electron diffraction. Reactor temperature, $T = 823, 853, 1113$ K; $S = (4\pi/\lambda)\sin \theta$, where λ is the electron wavelength and θ is the scattering angle.

Argon at the outlet of reactor. By contrast, the second regime corresponded to conditions that the cold-zone coagulation time $t_c = 6.3-62.4$ s was much larger than the reaction time $t_R = 0.5$ s. The fractal dimensions determined (for $T = 873$ K) were $D_f = 2.4$ and $D_f = 1.65$ for the first and the second regimes, respectively.

An important parameter to characterize the electronic and atomic structure of aerosol particles is the total number of chemically bonded hydrogen atoms.[37] Figure 3 shows the number of hydrogen atoms in particles versus reaction temperature. For comparison, Figure 4 reports the profiles of scattered electron intensity obtained by an transmission electron microscope operating in the regime of electron diffraction for different reaction temperatures.

Agglomerates of aerosol particles deposit on the surfaces of tubes through which a flow with aerosol is coming (both in the reactor hot zone and downstream). As a result, some loose deposited matter is formed at the surface. Figure 5 shows that such a deposit consists of some chains, tendrils, and tentacles. To better understand the mechanism of coagulation, we first observed the mechanism of the sticking of the free agglomerates to the tendrils, which constitute the deposit on the surface. To this end, a quartz filament was fixed inside of the imaging system probe volume. The injected aerosol formed a deposit at the surface of this filament. Then, the free agglomerate was observed sticking to the tendrils. The process is represented in Figure 6 by six frames, each recorded at a time lag 0.04 s with respect to the previous one. Figure 7 represents the time plot of the distance observed between the tendril and the agglomer-
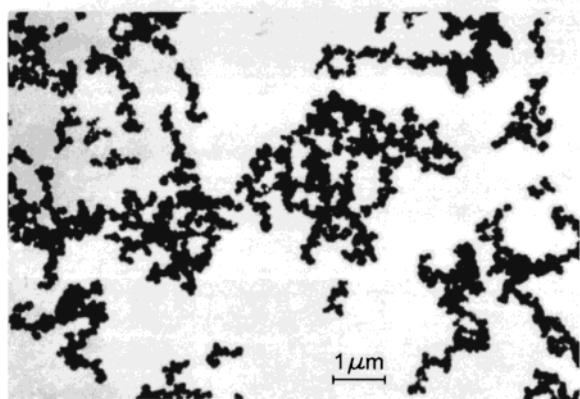
Evidence for Long-Range Coulomb Effects

J. Phys. Chem. A, Vol. 104, No. 45, 2000 **10429**

Figure 5. TEM image of a fragment of deposit sampled from the reactor surface at the reaction zone near the outlet.

Figure 7. The distance between the silicon agglomerate and the tendril (presented in Figure 6) vs time.

Figure 6. Imaging system results, illustrating silicon agglomerate–tendril collisions. The picture is represented by a serie of frames separated by a time interval, $\Delta t = 0.04$ s. Time increases from top to bottom. Reactor temperature, $T = 873$ K. cold-zone coagulation time, $t = 10$ s.

Figure 8. Imaging system results illustrating collisions between silicon agglomerates. The picture is represented by a series of frames separated by a time interval, $\Delta t = 0.02$ s. Time increases from top to bottom. Reactor temperature, $T = 873$ K. Cold-zone coagulation time, $t = 10$ s.

ate. It is evident from the figure that the agglomerate velocity increases progressively with time, as effect of some attractive interaction between the agglomerate and the tendril.

Figure 8 illustrates collisions between two silicon agglomerates with mutual sticking at the agglomerate tips. The distance between the two agglomerates is plotted as a function of time in Figure 9. The relative velocity of the agglomerates approaching each other progressively increases with time. Thus, the velocity increase is the evidence that some attractive interactions
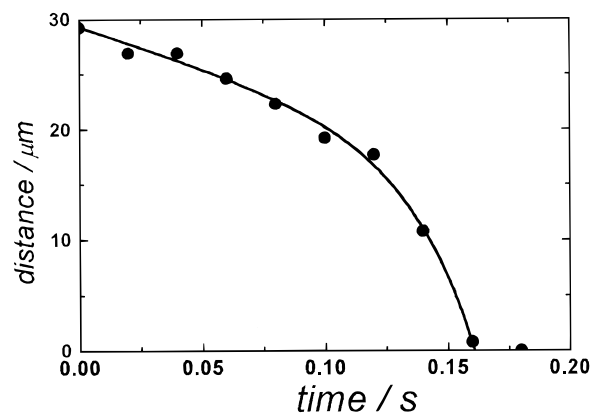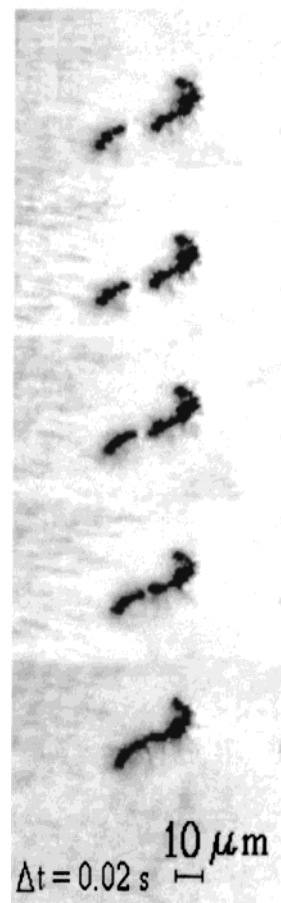
between agglomerates take place, just as in the situation described in Figure 7. Our observations of agglomerate-tendril and agglomerate-agglomerate collisions showed that reorientation of agglomerates does occur immediately before the sticking act, so that the agglomerates stick to each other by their tips (see, for example, Figure 8). This means that interactions between agglomerates lead to an enhancement of the formation of chainlike agglomerates with respect to the case of absence of such interactions. Thus, the resulting fractal dimension is lower (more open structure) with respect to the case of absence of such interactions.
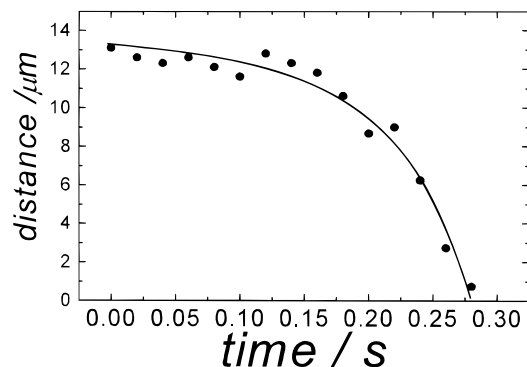
Figure 9. The distance between the silicon agglomerates (presented in Figure 8) vs time.

One of the ideas to justify the occurrence of tendril–agglomerate and agglomerate–agglomerate interactions is the possible role played by the electric charge on the agglomeration mechanism. To verify this hypothesis, we convoyed silicon agglomerates through a region where a homogeneous electric field was generated. In these experiments, the reaction time was 0.5 s, $T = 873$ K, and the cold-zone coagulation time was 10 s, which corresponded to the average radius of agglomerates $R \approx 0.5$ μm. The applied homogeneous electric field was 500 V/cm. After the injecting the aerosol probe into the volume, we did not find any drift of agglomerates in this field (with the accuracy of 3 μm/s). This means that, within the experimental error, we can conclude that the agglomerates are electrically neutral i.e., the net charge is equal to zero.

Another source of possible attractive interactions between agglomerates was thought to be the existence of a dipole moment of silicon agglomerates. To assess this point, we gathered agglomerates (after 10 s of cold-zone coagulation, reaction time $= 0.5$ s) into an inhomogeneous electric field, created by applying a voltage difference (1000 V) between a metal wire (diameter $= 0.03$ cm) and a (infinite in this geometry) metallic plate. The distance between the wire and the plate in this configuration was $d = 1.5$ cm, and the radius of the wire $r_0 = 1.5 \times 10^{-2}$ cm. A micro-objective lens was used to focus the plane (normal to the metal plate) containing the wire. Under these conditions, the agglomerates, within the space between the wire and the plate, were observed to move with acceleration in direction of the wire independently from polarity. At the distance of 0.04 cm from the surface of the wire, the arithmetic mean velocity of agglomerates was $v = 120$ μm/s for $T = 873$ K.

The movement of agglomerates in the inhomogeneous electric field can be explained by two physical mechanisms. One of them is the role played by the dipole moment induced by the electric field. The other mechanism is an intrinsic dipole moment of the agglomerate promoted by physical or chemical properties of primary particles. The acceleration to which two agglomerates are subjected during the sticking process (Figures 8 and 9) leads us to assumption that the reason for this interaction is an intrinsic dipole moment. To investigate this eventuality, we placed the agglomerates into an electric field and alternatively switched the polarity to the opposite sign. Thus, we observed that the agglomerates pivoted on themselves at the switching of electric field polarity. Figure 10 shows the sequence with such an agglomerate pivoting.

3.2. Soot Agglomerates. Figure 11 shows TEM micrographs of soot agglomerates sampled at different heights above burner (HAB). Figure 11a corresponds to HAB $= 2$ cm. Agglomerates formed by the assembly of primary particles and single particles
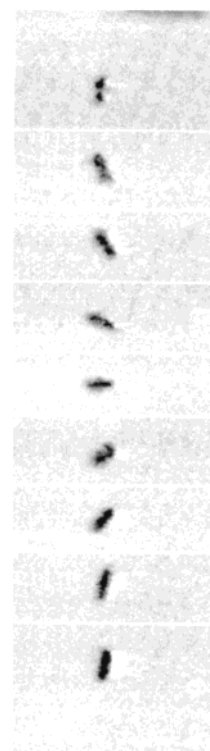

40 μm

$\Delta t = 0.02$ s

Figure 10. Series of frames illustrating the silicon agglomerate rotations after switching the electric field polarity to the opposite. The frames are separated by a time interval, $\Delta t = 0.02$ s. Time increases from top to bottom. Reactor temperature, $T = 873$ K.

could be observed. The size of primary particles is in the range of 10–25 nm. Figure 11b corresponds to the HAB $= 7$ cm. The primary particles comprising agglomerates in Figure 11b are considerably larger than those in Figure 11a. The reason for the presence of large sized primary particles at 7 cm HAB is the occurrence of a sintering process, i.e., adjacent primary particles in the same agglomerate merging together and form a unique primary particle. The analysis of the TEM micrographs showed that the average radius R of agglomerates increases from 40 to 70 nm when HAB is increasing from 2 to 7 cm.

We carried out experiments using the imaging system. First, we observed soot agglomerates sticking to the tendrils and tentacles composing the surface deposit. The sequence in Figure 12 demonstrates such a sticking. The mutual distance between the agglomerate and the tendril is given as a function of time in Figure 13. A strong attractive interaction was also observed in the case of the mutual approaching between a soot agglomerate and a tendril with a significant increase in agglomerate velocity with time.

The experiments were conducted by the application of a static electric field generated by a wire-metallic plate configuration similar to that described above. Direct agglomerate counting was performed by analyzing a sequence of frames shooting the movement of an ensemble of soot agglomerates in the presence of an applied electric field.
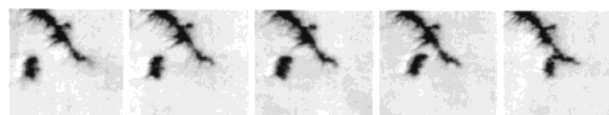
Evidence for Long-Range Coulomb Effects

J. Phys. Chem. A, Vol. 104, No. 45, 2000 **10431**
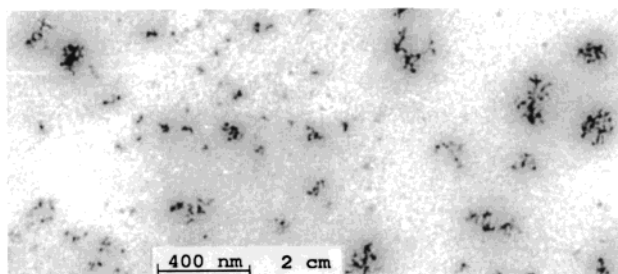
a
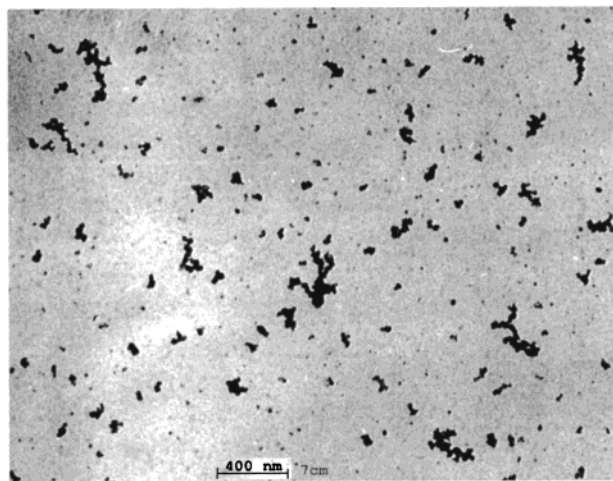
b

Figure 11. TEM micrographs of soot agglomerates sampled at hight above burner *a*, HAB = 2 cm; *b*, HAB = 7 cm.

$\Delta t = 0.04$ s   40 μm

Figure 12. Imaging system results illustrating soot agglomerate−tendril collisions. The picture is represented by a series of frames separated by a time interval of $\Delta t = 0.04$ s. Time increases from left to right.
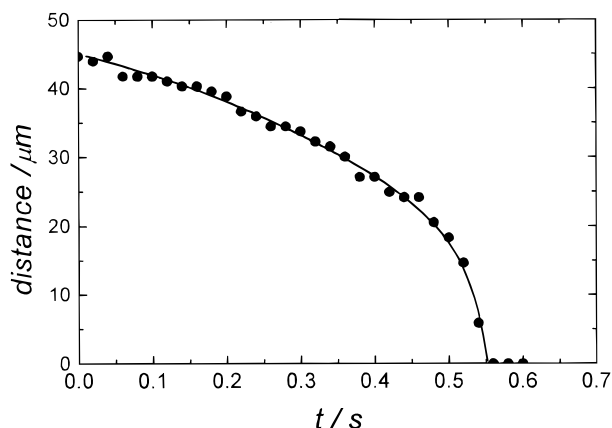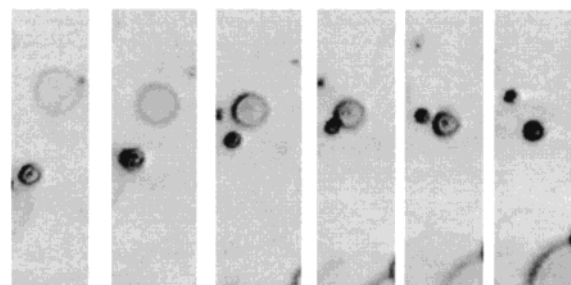

Figure 13. The distance between the soot agglomerate and the tendril (presented in Figure 12) vs time.

In particular, the wire/plate configuration was constituted by a wire with a diameter of 0.02 cm, positioned to a distance 1.0 cm from the plate. The movement of agglomerates in the electric field is illustrated by the eight frames (time lag 0.08 s) shown

$\Delta t = 0.08$ s   40 μm

Figure 14. Movement of the charged soot agglomerates in electric field. The frames are separated by the time interval of 0.04 s. The time increases from left to right.

in Figure 14. One of the agglomerates in Figure 14 was observed to move upward toward the negative electrode. Therefore, it was concluded that in this case, the agglomerate is carrying a positive net charge. Another agglomerate in the same Figure 14 was moving downward, and thus, it was retained to carry a negative net charge. When the polarity was switched, the agglomerates changed the direction of the movement. Direct counting from images allowed us to estimate not only the part of agglomerate population with net positive or negative charge but also the total fraction of agglomerates bringing a charge (positive or negative). To this end, counting was performed of the total number of agglomerates drifting both upward and downward. These estimations showed that about 50% of agglomerates carry a net charge. The reason for the agglomerates being charged lies in the ion formation during combustion process.[26−31] These ions could serve as centers of condensation[28−31] resulting in charged particle formation. Another possibility for charged particle formation could be the deposition of ions to neutral particles.

Also, in the case of soot agglomerates, the coagulation of bipolar charged aerosol was found to lead to eventual dipole agglomerate formation. By using the same imaging system described in section 2, we observed rotations of some agglomerates when changes in the polarity of the applied electric field were made (Figure 15).

4. Discussion

4.1. Mechanism of Silicon Particle Agglomeration. The experimental data presented in Section 3 showed that the agglomerates of aerosol particles formed by silane pyrolysis were dipoles. Then the question was, what is the cause of the dipole agglomerate formation ? We propose the following model. As mentioned in Section 3, aerosol particles formed under pyrolysis consisted of amorphous hydrogenated silicon. It is well-known that the atomic and electronic structures of amorphous silicon depend on the amount of bonded hydrogen present as a constituent of monohydride and polyhydride groups. Figures 3 and 4 demonstrate the existing correlation between the hydrogen contents of particles and the degree of ordering of amorphous networks. By comparison of Figures 3 and 4, it could be concluded that the higher the [H]/[Si] ratio, the more disordered the amorphous networks would become. For a reactor temperature $T = 823$ K, the ratio [H]/[Si] resulted about 0.45. The atomic structure of these particles was strongly disordered. As a matter of fact, no diffraction patterns were observed (Figure 4). For temperature $T = 853$ K, the ratio [H]/[Si] was about 0.15. For this temperature, Figure 4 demonstrated the occurring of peaks of amorphous silicon. Thus, in this case, the atomic structure of the amorphous silicon resulted in a more ordered
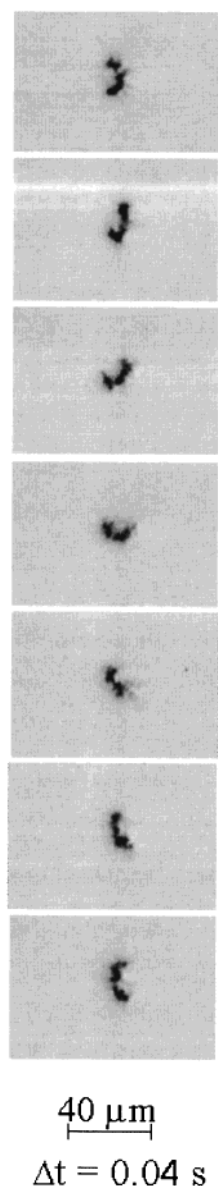
40 μm

Δt = 0.04 s

Figure 15. Series of frames illustrating the soot agglomerate rotations after the switching the electric field polarity to the opposite. The frames are separated by a time interval Δt (shown in the Figure). Time increases from top to bottom.

structure than that in the case of $T = 823$ K. At $T > 870$ K, the amount of bonded hydrogen was less than 5%, which is in agreement with Figure 4 showing polycrystalline structure of silicon at $T = 1113$ K.

Thus, inside the reactor hot zone, the particle population is characterized by different [H]/[Si] ratios. Some particles contain more hydrogen, other particles have less bonded H atoms. This means that the aerosol particles have different atomic and electronic structures. In other words, aerosol particles have different chemical potentials for electrons μ_e (different Fermi's energies). When two particles (with different μ_e) stick to each other in the hot zone, the electrons migrate from the region of higher chemical potential μ_e to the region of lower μ_e. The electrons migrate until the contact voltage compensates the difference in Fermi's energies. Thus, at the temporal stage before the occurring of chemical potential equalization, the particles (or agglomerates) were dipoles. However, the hydrogen atoms are usually very mobile at high temperatures. As a consequence of this, they migrate intensively through the silicon networks,[34] and therefore, the hydrogen concentration reaches equilibrium

very quickly over the particles. The effect of equilibration of hydrogen contents is to force to zero the dipole moment of the particles (or agglomerates). The equilibration time at $T = 873$ K is estimated to be about 5×10^{-4} s,[34] which is much shorter than the time between collisions of particles.

At the outlet of the reactor, the measured temperature was rapidly decreasing. Thus, hydrogen atoms became immobile,[34] and the collision of two particles (or agglomerates) with different μ_e results in dipole agglomerate formation. We refer to these initial dipole agglomerates as to the *primary dipoles*. Further downstream in the cold zone, a coagulation of dipole agglomerates takes place resulting in chainlike agglomerate formation.

It is crucial to stress that the fractal dimension for agglomerates formed in the hot zone was found to be $D_f \approx 2.4$, whereas for agglomerates formed in the cold zone, it was $D_f \approx 1.65$. One of the reasons for this difference in D_f is the restructuring of agglomerates in the hot zone. Another reason could be the Coulomb interactions between colliding agglomerates in the cold zone.

Let us estimate the agglomerate dipole moment p by using the inhomogeneous field experimental data. The motion equation reads

$$- p \frac{dE(r)}{dr} \approx F_M + M \frac{dv}{dt} \qquad (4)$$

The electric field $E(r)$ and force F_M are written as

$$E(r) = \frac{U}{\ln 2 + ln(d/r_0)} \times \left[\frac{1}{r} + \frac{1}{2d - r}\right] \qquad (5)$$

$$F_M = 6\pi R_m \eta v \gamma \qquad (6)$$

where R_m is the mobility radius, which is nearly equal to the radius of a sphere with the same projected area[7] (in ous case $R_m = 0.3$ μm), η is the coefficient of viscosity for Argon (2.25×10^{-4} Poise), r is the distance from the wire axis, v is the particle velocity ($v = 120$ μm/s for $r = 0.055$ cm), U is the voltage applied between the wire and the plate (1000 V), d is the distance from the wire axis to the plate (1.5 cm), r_0 is the radius of wire (1.5×10^{-2} cm), γ is a shape factor, which takes into account the fact that the agglomerates move along their longest axes. (As mentioned in Section 3.1, our agglomerates are characterized by the ratio $L/W = 1.9$. According to this ratio, we set $\gamma = 0.9$.)[39] The term $M\, dv/dt$ (M is the mass of agglomerate) was small with respect to the other terms, and it could be neglected. From the equations (4−6), we obtained the mean value of the agglomerate dipole moment $p = 6.6 \times 10^{-12}$ CGSE units. Our assumption was that the agglomerate dipole moment equals to the sum of dipole moments p_{pr} of primary dipoles. The fractal power law allows us to evaluate the number n_{pr} of the primary dipoles contained in the agglomerate

$$n_{pr} = (R/R_{pr})^{1.65} \qquad (7)$$

where R_{pr} and R are the radii of the primary dipole and agglomerate, respectively ($R_{pr} = 0.1$ μm, $R = 0.5$ μm). The estimation of primary dipole moment is $p_{pr} = 4.6 \times 10^{-13}$ units of CGSE.

The p_{pr} value could alternatively be evaluated by using the experimental data on agglomerate−agglomerate collisions (Figure 8). This computation gave $p_{pr} = 1.4 \times 10^{-13}$ units of CGSE, which is in reasonable agreement with the value $p_{pr} = 4.6 \times 10^{-13}$ units of CGSE obtained from the inhomogeneous field data.

Evidence for Long-Range Coulomb Effects

J. Phys. Chem. A, Vol. 104, No. 45, 2000 **10433**

It should be remembered that the dipole moment is induced when neutral particles are in the electric field. The induced dipole moment p_{ind} for agglomerates moving in the inhomogeneous electric field at the distance r from the wire axis (the agglomerates are oriented along the field), could be bounded by the following relationship

$$P_{ind} < (4\pi)^{-1} V_A(\epsilon - 1) E(r) \qquad (8)$$

where ϵ is the dielectric permittivity (we used the permittivity $\epsilon = 12$ for crystalline silicon as an upper limit), $E(r)$ is the electric field, V_A is the agglomerate volume. The agglomerate volume can be estimated from our empirical equation, obtained from TEM images: $V_A(\mu m^3) = 4.2 \times 10^{-2}[R(\mu m)]^{1.65}$. The estimation for the electric field E (see eq 5) calculated at $r = 5.5 \times 10^{-2}$ cm (i.e., for the distance at which the velocity was measured) gives $p_{ind} < 10^{-13}$ (units of CGSE) for the agglomerate radius $R = 0.5$ μm. The dipole moment, as determined by our experiments, is $p = 6.6 \times 10^{-12}$ units of CGSE. Thus, we conclude that the induced dipole moment is negligible compared to the experimentally determined dipole moment.

From the computation reported above, the dipole moment of the primary dipoles resulted in the range 1.4 to 4.6×10^{-13} (units of CGSE). Thus, the difference of the electric potential corresponding to the primary dipole moment could be estimated as the following

$$p_{pr}/L_{pr}^2 = (1.5-5) \times 10^{-4} \text{ (Units of CGSE)} = 0.05-0.15 \text{ V} \qquad (9)$$

where L_{pr} is the average length of the primary dipoles (equal to ~ 0.3 μm). This value seems quite reasonable because Fermi's energy fluctuations in coagulating particles can be as much as about 0.5 eV.[38]

We suggest that the phenomenon of dipole agglomerate formation due to coagulation of particles with different electronic structure is not restricted by silane thermal decomposition. There should be many other systems in which this effect plays a role. Dipole agglomerates are considered to be produced by a coagulation process occurring between both conductor and semiconductor particles with dispersion of electronic properties or by two- or multicomponent aerosol coagulation mechanism.

4.2. Estimation of Net Charge and Dipole Moment of Soot Agglomerates. Figure 14 shows the movement of two soot agglomerates with opposite charges in the presence of an applied electric field. The negative electrode was the wire. For our reference, the wire axis was positioned at a distance about 400 μm with respect to the center of each frame. The balance between the electrical force and drag force, eq 5, was written in this case as the following

$$neE(r) = 6\pi\eta v R_m \qquad (10)$$

where η is viscosity of the carrier gas (air in this case) equal to 1.85×10^{-4} Poise, v is the agglomerate velocity, R_m is the mobility radius. The r value was estimated for the agglomerate moving upward (first frame) and results about 400 μm. This configuration determines an electric field $E_w(r) \approx 13$ kV/cm. The agglomerate velocity, estimated from the two initial frames, is about 0.013 cm/s. The mobility radius is about 5 μm. The net charge evaluated by the application of eq 10 was therefore about one elementary unit.

The experimental data presented in Section 3 shows that the coagulation of charged agglomerates could result in dipole agglomerate formation. It was significant to estimate the dipole moment of the soot agglomerate represented in the Figure 15. The agglomerate rotation due to the moment of external force is governed by the equation

$$d\theta/dt = B_\omega M_\theta \qquad (11)$$

where θ is rotation angle, B_ω is the "rotational mobility", M_θ is a moment of external force. To evaluate the dipole moment, the agglomerate shown in Figure 15 was considered as an ellipsoid of revolution with the ratio of the longest axis to the smaller one $\beta = 6$. In this case:[39]

$$B_\omega = 5.9(\pi\eta L^3)^{-1} \qquad (12)$$

where L is the length of agglomerate. From Eqs 11 and 12, the dipole moment p resulted as 9.6×10^{-13} (units of CGSE). This dipole moment was found to correspond to a configuration in which two elementary charges of opposite signs are located at a distance of 20 μm, which was in very nice agreement with the real length of the agglomerate observed (Figure 15).

5. Conclusions

The Coulomb interactions between the coagulating particles were investigated under the agglomeration of primary nanoparticles synthesized in silane pyrolysis and propane-air combustion processes. The nature of these electric interactions was found to be different in each of the considered process. In the case of silane pyrolysis, a coagulation of agglomerates took place in which agglomerates behaved as electric dipoles. The cause of the formation of dipole agglomerates was individuated to probably be the difference of chemical potential for electrons in different primary particles. In the case of soot formation, approximately half of the total agglomerate number was evaluated to be carrier of net charge about unity, with both positive and negative sign. As a consequence of the coagulation process occurring between charged particles, some soot agglomerates were dipoles. In an exemplary case, shown in the paper, the computed value of dipole moment for a theoretical configuration of two elementary charges (positive and negative) at a mutual distance equal to the real agglomerate length, resulted in very nice agreement with the measured dipole moment inferred from the rotation mobility of soot agglomerates observed in the experiments in the presence of an applied electric field.

References and Notes

(1) Ehrmann, S. H.; Friedlander, S. K.; Zachariah, J. *Aerosol Sci.* **1998**, *29*, 687.

(2) Jang, H. D.; Friedlander, S. K. *Aerosol Sci. Technol.* **1998**, *29*, 81.

(3) Kobata, A.; Kusakabe, K.; Morooka, S. *AIChE Journal* **1991**, *37*, 347.

(4) Morooka, S.; Yasutake, T.; Kobata, A.; Ikemizu, K.; Kato, Y. *Int. Chem. Eng.* **1989**, *29*, 119.

(5) Okuyama, K.; Kousaka, Y.; Tohge, N.; Yamamoto, S.; Wu, J. J.; Flagan, R. C.; Seinfeld, J. H. *AIChE Journal* **1986**, *32*, 2010.

(6) Rogak, S. N.; Baltensperger, U.; Flagan, R. C. *Aerosol Sci. Tech.* **1991**, *14*, 447.

(7) Rogak, S. N.; Flagan, R. C.; Nguyen, H. V. *Aerosol Sci. Tech.* **1993**, *18*, 25.

(8) Hurd, A. J.; Flower, W. L. *J. Colloid Interface Sci.* **1988**, *122*, 178.

(9) Martin, J. E.; Schaefer, D. W.; Hurd, A. J. *Phys. Rev. A* **1986**, *33*, 3540.

(10) Ulrich, G. D.; Riehl, J. W. *J. Colloid Interface Sci.* **1982**, *87*, 257.

(11) Samson, R. J.; Mulholland, G. W.; Gentry, J. W. *Langmuir* **1987**, *3*, 272.

(12) di Stasio, S. *J. Aerosol Sci.* **1999**, *30*, *S1*, 325.

(13) di Stasio, S. *Appl. Phys. B.* **2000**, *70*, 635.

(14) Zhang, H. X.; Sorensen, C. M.; Ramer, E. R.; Olivier, B. J.; Merklin, J. F. *Langmuir* **1988**, *4*, 867.

(15) Meakin, P. *Phys. Rev. A* **1984**, *29*, 997.

(16) Raymond, F.; Mountain, D.; George, W.; Mulholland, W.; Baum, H. *J. Colloid Interface Sci.* **1986**, *114*, 67.

(17) Julien, R.; Meakin, P. *J. Colloid Interface Sci.* **1989**, *127*, 265.

(18) Witten, T. A.; Sander, L. M. *Phys. Rev. Lett.* **1981**, *47*, 1400.

(19) Mulholland, G. W.; Samson, R. J.; Mountain, R. D.; Ernst, M. H. *Energy Fuels* **1988**, *2*, 481.

(20) Richter, R.; Sander, L. M.; Cheng, Z. *J. Colloid Interface Sci.* **1984**, *100*, 203.

(21) Rogak, S. N.; Flagan, R. C. *Part. Syst. Charact.* **1992**, *9*, 19.

(22) Sutherland, D. N.; Goodarz-Nia, I. *Chem. Eng. Sci.* **1971**, *26*, 2071.

(23) Tolman, S.; Meakin, P. *Rhys. Rev. A* **1989**, *40*, 428.

(24) Meakin, P.; Witten, T. A., Jr. *Phys. Rev. A* **1983**, *28*, 2985.

(25) Meakin, P. *J. Chem. Phys.* **1984**, *81*, 4637.

(26) Ball, R. T.; Howard, J. B. Electric Charge of Carbon Particle in Flames: *13th International Symposium on Combustion*, 353, The Combustion Institute, 1971.

(27) Wersborg, B. L.; Howard, J. B.; Williams, G. C. Physical Mechanisms in Carbon Formation in Flames: *14th International Symposium on Combustion*, 929, The Combustion Institute, 1973.

(28) Howard, J. B. On the Mechanism of Carbon Formation in Flames: *12th International Symposium on Combustion*, 877, The Combustion Institute, 1969.

(29) Place, E. R.; Weinberg, F. J. *Proc. R. Soc., A* **1966**, *289*, 192.

(30) Lahaye, J.; Prado, G. In *Chemistry and Physics of Carbon*; Marcel Dekker: New York, 1978.

(31) Palmer, H. B.; Cullis, C. F. In *Chemistry and Physics of Carbon*; Marcel Dekker: New York, 1965.

(32) Onischuk, A. A.; Strunin, V. P.; Ushakova, M. A.; Panfilov, V. N. *J. Aerosol Sci.* **1997**, *28*, 207.

(33) Onischuk, A. A.; Strunin, V. P.; Samoilova, R. I.; Nosov, A. V.; Ushakova, M. A.; Panfilov, V. N. *J. Aerosol Sci.* **1997**, *28*, 1425.

(34) Onischuk, A. A.; Samoilova, R. I.; Strunin, V. P.; Chesnokov, E. N.; Musin, R. N.; Bashurova, V. S.; Maryasov, A. G.; Panfilov, V. N. *Appl. Magn. Res.* **1998**, *15*, 59.

(35) Onischuk, A. A.; Strunin, V. P.; Ushakova, M. A.; Panfilov, V. N. *Phys. Stat. Sol. B* **1994**, *186*, 43.

(36) Onischuk, A. A.; Strunin, V. P.; Ushakova, M. A.; Samoilova, R. I.; Panfilov, V. N. *Phys. Stat. Sol. B* **1996**, *193*, 25.

(37) Allan, D.; Joannopoulos, J. D. In *The Physics of Hydrogenated Amorphous Silicon (II)*; Joannopoulous, J. D., Lucovsky, G., Eds.; Springer-Verlag: Berlin, 1984.

(38) Mott, N. F.; Davis, E. A. In *Electron Processes in Non-Crystalline Materials*; Clarendon Press: Oxford, 1979.

(39) Fuchs, N. A. In *The Mechanics of Aerosols*; Pergamon Press: Oxford, 1964.